

Wire-Level Interrupt-to-Decision Latency of On-Sensor MLC versus Host Inference on the NVIDIA Jetson Orin Nano: A Pre-Registered Measurement Study

Akul Swami¹ and Dnyaneshwar Sonawane²

¹Independent Researcher (e-mail: swami.akul@alumni.uml.edu)

²Independent Researcher (e-mail: sonawane.dnyaneshwar19@gmail.com)

Manuscript submitted May 28, 2026.

Abstract—The Machine Learning Core (MLC) embedded in the STMicroelectronics LSM6DSOX IMU is widely cited as a low-latency alternative to host-side inference, yet wire-level decision-delivery latency is rarely measured. Using a Saleae Logic Pro 8 logic analyzer on an NVIDIA Jetson Orin Nano, we measured interrupt-to-decision latency (sensor INT1 edge to host decision GPIO) for three pipelines (a host-side decision-tree classifier, the standard MLC bank-switch read protocol, and an MLC binary-fast variant) under idle, I²C bus contention, and CPU stress. The protocol was pre-registered with 12 externally-timestamped Zenodo amendments before confirmatory data collection (4,770 of 4,860 trials included, 98.15%, across nine cells). The host pipeline exhibits lower median latency than the MLC pipeline under all conditions: 321.7 vs 681.5 μ s at idle (2.1 \times faster) and 574.5 vs 1,325.4 μ s under I²C contention (2.3 \times faster). The three-transaction I²C read protocol, not the silicon’s classification, is the dominant latency contributor. We additionally characterize a reproducible 706.5 ms MLC decision cadence that bounds full stimulus-to-decision latency. Code, data, and pre-registration: github.com/akulswami/sensor-mlc-latency.

Index Terms—Inertial measurement unit, machine learning core, edge inference, latency measurement, pre-registration, LSM6DSOX.

I. INTRODUCTION

Inertial measurement units (IMUs) with embedded Machine Learning Cores (MLCs) are increasingly deployed in edge applications spanning wearables, industrial monitoring, and biomedical instrumentation [1]. The MLC paradigm runs a decision-tree classifier inside the sensor and exposes only an output register to the host. It is often framed as a latency and energy advantage over host-side classification [2], [3], on the implicit assumption that on-sensor inference is unconditionally lower-latency because the host need only poll a single register.

This assumption is rarely tested with wire-level instrumentation. Vendor application notes characterize MLC architecture and per-class accuracy but not end-to-end stimulus-to-decision latency [2]. Even recent safety-critical applications such as exoskeleton control [3] cite the on-sensor latency advantage without measuring it directly. The resulting gap between “the classification is correct” and “the classification reaches the host in time to act” is the failure mode conventional functional testing misses.

We measure wire-level interrupt-to-decision latency (sensor INT1 edge to host decision GPIO) for three pipelines on a representative edge platform (NVIDIA Jetson Orin Nano + STMicroelectronics LSM6DSOX over I²C) using a Saleae Logic Pro 8 logic analyzer: (a) a host-side decision-tree classifier reading raw accelerometer data, (b) the standard MLC bank-switch read protocol, and (c) an MLC binary-fast variant that omits the I²C read entirely, toggling the decision GPIO on every MLC interrupt (valid for a 2-class configuration).

Measurements span idle, I²C bus contention, and CPU saturation. The full protocol was pre-registered with 12 externally-timestamped Zenodo amendments before confirmatory data collection [4].

The principal finding is that the host pipeline exhibits lower median wire-level latency than the standard MLC bank-switch pipeline under all tested conditions, with the three-transaction I²C read protocol, not the silicon’s classification, as the dominant latency contributor. Our contributions are: (1) the first pre-registered wire-level latency characterization of the LSM6DSOX MLC versus host-side inference (4,770 of 4,860 trials included, 98.15%, across nine pipeline \times condition cells); (2) empirical identification of the I²C read-protocol overhead as a dominant contributor on this platform, with structural relevance to systems using bank-switched register access for on-sensor ML output; (3) characterization of a reproducible 706.5 ms MLC decision cadence (one quarter of the 75-sample \times 26 Hz window) that bounds full stimulus-to-decision latency; and (4) pre-registration with externally-timestamped Zenodo DOIs as an audit-defensible framework for sensor-measurement claims.

II. BACKGROUND AND RELATED WORK

A. On-sensor inference in MEMS IMUs

Embedded machine learning in 6-axis microelectromechanical systems (MEMS) IMUs is now a standard product feature. STMicroelectronics introduced the MLC in the LSM6DSOX [2], a configurable decision-tree engine running at the accelerometer ODR (26 Hz in our deployment) that consumes features over sliding sample windows and emits class labels the host reads via I²C bank-switched registers. Successor parts (LSM6DSV16X [3], LSM6DSO32X) retain this architecture, and competing vendors offer analogues (Bosch BHI260AP, Analog Devices ADXL367). The consistent commercial messaging is that on-sensor inference reduces data-bus traffic, host

Corresponding author: A. Swami (e-mail: swami.akul@alumni.uml.edu). Code, data, and the full pre-registration chain are available at <https://github.com/akulswami/sensor-mlc-latency>.

This work has been submitted to the IEEE for possible publication. Copyright may be transferred without notice, after which this version may no longer be accessible.

CPU utilization, and end-to-end latency. The first two claims are testable from system-level metrics; the third is testable only with wire-level instrumentation, which is rarely performed.

B. Wire-level latency in safety-critical edge ML

A growing class of edge-AI applications depends on bounded stimulus-to-actuation latency: wearable exoskeleton control [3], industrial predictive-maintenance alarms, healthcare arrhythmia and fall detection. In each, “the classification is correct” is necessary but not sufficient; “the classification reaches the actuator in time” is the safety-relevant property. Yet vendor application notes report MLC architecture and accuracy without end-to-end latency [2], and independent characterizations measure host-side interrupt-to-action latency without measuring how the read protocol contributes to the wire-level delay. That gap, between functional and timing correctness, is the failure mode conventional functional testing misses.

C. Pre-registration in sensor measurement

Pre-registration, the externally-timestamped specification of hypotheses, exclusion criteria, tests, and multiplicity correction before data collection, is established in clinical trials and common in psychology and machine learning but rare in sensor measurement. We apply it here: externally-timestamped Zenodo DOIs provide a chain of custody distinguishing pre-specified hypotheses from post-hoc rationalization, with all methodology changes recorded as dated amendments against the public repository.

III. EXPERIMENTAL SETUP

A. Hardware Platform

The edge platform is an NVIDIA Jetson Orin Nano Developer Kit (JetPack 6.2.2, kernel 5.15.148-tegra, 6-core ARM Cortex-A78AE). All measurements ran under a custom MAXN_SUPER_JC nvpmode (v7.6 [4]) pinning all six CPUs at 1728 MHz; per-block jetson_clocks effectiveness (tegrastats samples ≥ 1700 MHz) was $\geq 99\%$, with all 81 blocks at 100%.

The sensor is an STMicroelectronics LSM6DSOX 6-axis IMU breakout (STEVAL-MKI197V1) on I²C bus 7 (pins 3/5, address 0x6A), the bus running at 400 kHz (Fast Mode, Jetson default). All three pipelines configure the accelerometer identically (CTRL1_XL = 0x50: 208 Hz, ± 2 g, LPF2 off). The MLC runs at 26 Hz with a custom 2-class motion/still classifier (75-sample windows, config mlc_motion_w75.h) trained in ST MEMS Studio, with output routed to INT1.

Two Jetson GPIO lines are instrumented with a Saleae Logic Pro 8 (250 MS/s): **D0** on pin 15 (INT1 from the LSM6DSOX, gpiochip0 line 85) and **D1** on pin 11 (decision edge from the pipeline under test, line 112). This yields nanosecond-resolution wire-level timestamps independent of the Jetson clock and of SSH command jitter (both D0 and D1 are wire edges). The wire-level GPIO timestamping methodology follows our prior cross-platform characterization [9]. Motion stimulus is an SG90 servo on a PCA9685 PWM controller (I²C bus 1, address 0x41 via an A0 solder bridge to avoid the on-board INA3221 at 0x40), commanded over SSH.

B. Pipelines Under Test

Three pipelines are compared end-to-end, sharing the same I²C arbitration, gpiod write path, and accelerometer configuration, and differing only in what happens after an interrupt arrives:

(a) **host** (host_pipeline_parity): polls the accelerometer at 208 Hz, assembles a 75-sample window, and applies a decision-tree classifier (variance of accelerometer L2-norm against a calibrated threshold), toggling D1 on every output state change.

(b) **mlc** (latency_test_mlc_w75): on each INT1 edge, performs the three I²C transactions of the bank-switch read (write FUNC_CFG_ACCESS = 0x80 to enter the embedded bank, read MLC0_SRC = 0x70, write FUNC_CFG_ACCESS = 0x00 to return), writing D1 if the output changed.

(c) **mlc-binary** (latency_test_mlc_binary_w75): on each INT1 edge, unconditionally toggles D1 without reading MLC0_SRC, valid for the 2-class case and providing a kernel/gpiod-only latency floor against which (b)’s I²C-read overhead is measured. Because this study measures decision-delivery latency rather than classification accuracy, parity is enforced at the level of identical accelerometer configuration, window length, and binary motion/still decision semantics; the mlc-binary condition isolates the non-classifier read path.

C. Stress Conditions

Three conditions are tested. **idle**: CPUs pinned but otherwise unloaded. **i2c-contention**: three concurrent i2c_hammer processes continuously read non-MLC registers from the LSM6DSOX on bus 7, contending for bus access. **stress**: stress-ng 0.13.12 saturates all six CPUs (`-cpu 6 -cpu-method matrixprod`). Hammer-process count and CPU saturation are verified at block start.

D. Measurement Protocol

Each (pipeline, condition) cell comprises 9 blocks of 300 s. Block order across the 81-block campaign follows a pre-registered deterministic shuffle (seed 1990185399 [4]). Within each block the orchestrator delivers 60 candidate transitions; latency is $t(D1) - t(D0)$. Inclusion (pre-registered v7.4) requires exactly one D1 rising edge per stimulus window; violations are categorized and reported as a classifier-stability outcome (Section V.D). Across the campaign, 4,770 of 4,860 trials (98.15%) were included, no cell exceeding the pre-registered 10% exclusion ceiling.

IV. METHODOLOGY AND STATISTICAL TREATMENT

A. Pre-registration

All hypotheses, exclusion criteria, statistical tests, and multiplicity-correction strategies were specified in a public, version-controlled pre-registration with externally-timestamped Zenodo DOIs [4]. The chain contains 12 substantive amendments (v6.1–v7.10); each was minted as a Zenodo release on the same calendar day as its git tag, giving an audit-defensible timestamp ordering. Three pre-registered hypotheses were falsified during the study and remain on the public record rather than being removed. H1 (MLC faster than host at idle) and H4’ (MLC idle energy below host) were falsified at pilot scale before the confirmatory campaign, prompting the reframing recorded in v7.5 and v7.6; H7’ (MLC stability degrades under I²C contention) was falsified by the confirmatory campaign itself (v7.10),

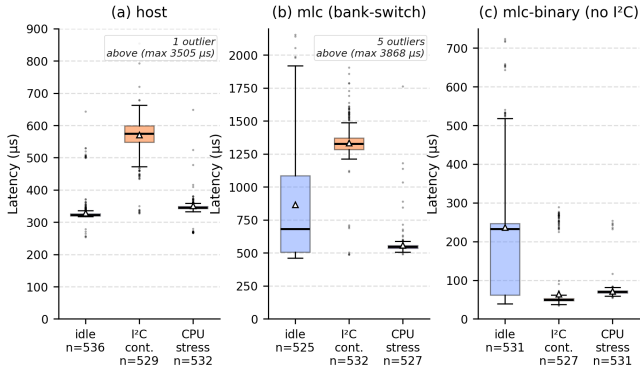


Fig. 1. Per-trial wire-level latency by pipeline and condition. The mlc-binary panel (zero I²C transactions on the decision path) isolates the kernel/gpiod latency floor; note the per-panel y-axis scaling. Box = IQR (Q1–Q3); whiskers = 1.5×IQR; Δ = mean; \bullet = outlier; y-axes are capped per panel, with outliers above each cap noted in-panel.

with the observed direction opposite to the prediction. Because each amendment is dated before the data it concerns, the chain distinguishes pre-specified predictions from outcomes rather than retrofitting hypotheses to results.

B. Statistical tests and multiplicity correction

Each hypothesis is matched to a pre-registered test. H1' and H2' (stochastic ordering of two independent samples) use a one-sided Mann-Whitney U test, with the Hodges-Lehmann shift and a 95% percentile-bootstrap CI (10,000 resamples) as the effect estimate [5], [6]. H3' (the interaction contrast $\Delta_{\text{MLC}} - \Delta_{\text{host}} > 0$) bootstraps the contrast statistic (10,000 resamples). H5' (equivalence within $\pm 30 \mu\text{s}$) uses TOST [7]: the 90% CI on the median difference must lie strictly within $[-30, +30] \mu\text{s}$. H6' (energy difference $> 1,000 \text{ mW}$) uses Mann-Whitney U on VDD_IN samples with 1/10 subsampling to reduce the autocorrelation of 100 ms-cadence INA3221 readings. H7' (stability ordering) uses a one-sided Fisher's exact test, chosen over chi-square because the per-cell unstable counts (6–15 of 540) fall where the chi-square asymptotic approximation is unreliable.

Multiplicity correction across the H1', H2', H3', H6', H7' family is by Holm-Bonferroni at family-wise $\alpha = 0.05$ [8]. H5' uses TOST equivalence rather than a directional p-value and is reported alongside the family rather than within it; this is an analysis-side refinement of the v7.5 specification, which had named a six-hypothesis Holm family.

V. RESULTS

The confirmatory campaign collected 4,860 candidate trials across 81 blocks of 300 s; 4,770 (98.15%) satisfied the pre-registered inclusion criteria. All blocks achieved 100% jetson_clocks effectiveness under MAXN_SUPER_JC. Per-cell latency distributions appear in Fig. 1; summary statistics in Table I.

A. Confirmatory tests

H1' (host < MLC at idle): SUPPORTED. Host idle median (321.7 μs) is 359 μs below MLC bank-switch idle (681.5 μs), a 2.1× host speedup. The Hodges-Lehmann shift is $\Delta\text{HL} = -359.3 \mu\text{s}$, 95%

TABLE 1. Wire-Level Latency per Pipeline × Condition (μs)

Pipeline	Condition	n	Median (μs)	IQR (μs , p25–p75)
host	idle	536	321.7	319.7–326.4
host	i2c-cont.	529	574.5	547.8–599.0
host	stress	532	345.0	342.0–349.0
mlc	idle	525	681.5	505.4–1086.8
mlc	i2c-cont.	532	1325.4	1283.8–1371.5
mlc	stress	527	546.1	535.8–557.0
mlc-binary	idle	531	231.9	61.8–246.2
mlc-binary	i2c-cont.	527	49.4	46.9–53.2
mlc-binary	stress	531	70.2	66.9–73.0

bootstrap CI $[-373.6, -352.5]$ (10,000 iterations); Mann-Whitney $p = 1.87 \times 10^{-170}$, rejected at the Holm-Bonferroni threshold across the H1', H2', H3', H6', H7' family.

H2' (host < MLC under I²C contention): SUPPORTED. With three concurrent i2c_hammer processes on bus 7, host median rises to 574.5 μs and MLC to 1,325.4 μs ; the shift grows to $\Delta\text{HL} = -753.2 \mu\text{s}$ $[-760.0, -746.7]$ (2.3× advantage), $p = 2.33 \times 10^{-170}$.

H3' (MLC degrades more than host): SUPPORTED. The Δ -of- Δ contrast is +391.1 μs [+372.8, +400.0], $p = 1.00 \times 10^{-4}$. The MLC degrades by +611.7 μs (+90%, idle→contention) versus the host's +249.2 μs (+78%): the MLC's three-transaction I²C read protocol amplifies the contention penalty.

H5' (CPU stress null for host latency): SUPPORTED. Host median rises only from 321.7 μs (idle) to 345.0 μs (stress); a TOST against the pre-registered $\pm 30 \mu\text{s}$ margin gives +23.3 μs , 90% CI $[+22.7, +23.7] \subset [-30, +30]$. Equivalence is declared; a 208 Hz polling loop does not contend with stress-ng for CPU time.

H6' (CPU stress positive for energy): SUPPORTED. Mean VDD_IN (INA3221 via tegrastats) rises from 5,206 mW (idle) to 8,626 mW (stress): +3,420 mW [+3,410, +3,429], exceeding the pre-registered +1,000 mW threshold threefold. The power axis distinguishes CPU stress unambiguously where the latency axis (H5') cannot.

H7' (MLC stability degrades under contention): FALSIFIED, direction opposite. The fraction of stimulus windows with exactly one D1 rising edge is 97.22% (525/540) at idle versus 98.89% (534/540) under contention, a +1.67 percentage-point *increase* rather than the predicted decrease. Fisher's exact test in the pre-registered direction gives $p = 0.9874$ (two-sided $p = 0.0755$). H7' is formally falsified in pre-registration v7.10 [4]. I²C contention slows the MLC pipeline (H2', H3') but does not degrade the silicon's classifier reliability.

B. Multimodal latency distributions

Fig. 1 reveals multimodal structure in both MLC pipelines. The mlc/idle distribution is bimodal (mean 866.6 μs exceeds median 681.5 μs , with p95 reaching 1,780.7 μs), and mlc-binary/idle shows three modes near 60, 240, and 470 μs . Under contention and stress both collapse to tighter distributions, consistent with idle-state variance reflecting the kernel/I²C scheduler's full timing-edge variability when not load-pinned. We report this as exploratory; the mechanism requires kernel-level (ftrace) instrumentation beyond this study's scope.

C. MLC decision cadence

Inter-trial D0 (INT1) gaps ($n = 3,086$) cluster sharply at integer multiples of $T = 706.5 \text{ ms}$ with empty inter-peak bins. T is consistent

with approximately one-quarter of the MLC’s 75-sample, 26 Hz window period ($2.885 \text{ s} / 4 = 0.721 \text{ s}$; empirical peak 0.7065 s , a 2% difference). In this configuration, the quantization is consistent with the MLC updating only on its internal window-cadence clock rather than the host read path; we did not find it described in ST application notes [2] or the LSM6DSOX datasheet.

D. Exclusion rates

No cell exceeded the pre-registered 10% exclusion ceiling (highest: *mlc/idle*, 2.78%). The dominant exclusion category (68 of 90 trials) was multiple D1 edges per window, attributable to the 706.5 ms cadence interacting with stimulus-window boundaries.

VI. DISCUSSION

A. The I²C read protocol dominates wire-level latency

The headline finding, that host classification is 2.1–2.3× faster than the on-sensor MLC under every tested condition, is explained by **Fig. 1(c)**: the *mlc*-binary pipeline, which performs zero I²C transactions on the decision path (toggling D1 unconditionally on every INT1 edge), reaches a median of $49.4 \mu\text{s}$ under contention. The *mlc*-minus-*mlc*-binary difference under identical conditions isolates the I²C read overhead at roughly $1,276 \mu\text{s}$ under contention ($1,325.4 - 49.4$) and $476 \mu\text{s}$ under stress. This cost is not the silicon’s classification time; it is the bank-switch read protocol’s three-transaction sequence (write `FUNC_CFG_ACCESS`, read `MLC0_SRC`, write it back) competing for bus arbitration.

Two consequences follow. Any platform using the LSM6DSOX MLC over I²C inherits this overhead by construction: the bank-switch protocol is neither optional nor bypassable on the standard read path. And the overhead scales with bus contention, not classifier complexity: a deeper decision tree would not change the per-decision I²C cost, but a busier bus would. The host-MLC gap is overwhelmingly a bus-protocol artifact, not a classifier-architecture one.

B. Implications for safety-critical edge ML

A naive reading of “on-sensor inference is faster” would favor the MLC for low-latency safety-critical loops such as exoskeleton control [3]. Our results invert that on the wire-level latency axis: the host reaches its decision $359 \mu\text{s}$ earlier at idle, $753 \mu\text{s}$ earlier under contention, and is equivalence-null against CPU stress (H5’).

The control results sharpen the practical lesson: **“stress” is not a single thing**. CPU stress is significant on energy (H6’, +3,420 mW) but null on host latency (H5’) and on classifier reliability; I²C bus contention is significant on latency (H2’, H3’) but null on classifier reliability (H7’ falsified; the stable-trial rate is, if anything, slightly higher under contention). A specification bundling both into one “stress margin” over-provisions one axis while under-provisioning the other.

C. Multimodal distributions and decision cadence

Two secondary findings carry safety-critical weight. First, the MLC pipelines are multimodal at idle (Section V.B): the *mlc/idle* p95 of $1,781 \mu\text{s}$ is 2.6× its median, a factor that vanishes under a unimodal-Gaussian assumption. For a “worst latency observed with probability

$1 - \varepsilon$ ” specification, the upper mode, not the median, is the relevant quantity.

Second, for unsynchronized external stimuli, the observed 706.5 ms cadence (Section V.C) can dominate full *stimulus-to-decision* latency at the system level. Because the MLC fires only on its internal clock boundary, an unsynchronized real-world stimulus waits a uniformly-distributed 0–706.5 ms (mean 353 ms) before the silicon can respond. This is invisible on the D0-to-D1 wire-level axis we measured but is a structural floor; the 1–2 ms wire-level differences this paper characterizes are second-order against it.

D. Limitations

Results are specific to one platform, sensor IC family, bus protocol (I²C, not SPI), ODR, and MLC configuration; the structural findings should transfer to similar ARM-edge + ST-MEMS combinations but require confirmation. SPI access in particular could reduce the per-transaction overhead that drives our result. A pre-registered RT-scheduling (`chrt+taskset`) ablation was specified but not activated; pilot data suggest it could roughly halve MLC contention latency, making it the most concrete next step.

VII. CONCLUSION

We measured wire-level interrupt-to-decision latency for three pipelines on a Jetson Orin Nano + LSM6DSOX edge platform. Against the intuition that on-sensor inference is faster, the host pipeline achieves 2.1× lower median latency at idle and 2.3× lower under I²C contention; the *mlc*-binary variant isolates the bank-switch read protocol’s $1,276 \mu\text{s}$ contention cost. The three-transaction I²C read, not the silicon’s classification, dominates. The control results show that which resource is contended is itself the safety-critical variable: CPU stress registers on energy but not latency, while I²C contention does the reverse. We document a reproducible 706.5 ms MLC decision cadence imposing a 0–706.5 ms stimulus-to-decision wait for unsynchronized stimuli.

REFERENCES

- [1] STMicroelectronics, “LSM6DSOX: 6-axis IMU with machine learning core,” Datasheet DS12140, 2024.
- [2] STMicroelectronics, “LSM6DSOX: Machine Learning Core,” Application Note AN5259, 2023.
- [3] M. Razmi and I. Shojaei, “Event-driven on-sensor locomotion mode recognition using a shank-mounted IMU with embedded machine learning for exoskeleton control,” arXiv:2602.21418, Feb. 2026.
- [4] A. Swami, “Pre-registration chain for the sensor-mlc-latency study,” Zenodo, externally-timestamped multi-amendment DOI chain (v6.1–v7.11), 2026. doi:10.5281/zenodo.20437893 (v7.11).
- [5] H. B. Mann and D. R. Whitney, “On a test of whether one of two random variables is stochastically larger than the other,” *Ann. Math. Statist.*, vol. 18, no. 1, pp. 50–60, 1947.
- [6] J. L. Hodges and E. L. Lehmann, “Estimates of location based on rank tests,” *Ann. Math. Statist.*, vol. 34, no. 2, pp. 598–611, 1963.
- [7] D. J. Schuurmann, “A comparison of the two one-sided tests procedure and the power approach for assessing the equivalence of average bioavailability,” *J. Pharmacokin. Biopharm.*, vol. 15, no. 6, pp. 657–680, 1987.
- [8] S. Holm, “A simple sequentially rejective multiple test procedure,” *Scand. J. Statist.*, vol. 6, no. 2, pp. 65–70, 1979.
- [9] A. Swami and N. Chougule, “Per-platform GPIO overhead in hardware-validated edge ML inference timing,” arXiv:2605.02835, May 2026.